Two-dimensional Stokes flow driven by elliptical paddles

Stephen M. Cox[a)]
School of Mathematical Sciences, University of Nottingham, Nottingham NG7 2RD, United Kingdom

Matthew D. Finn[b)]
School of Mathematical Sciences, University of Adelaide, Adelaide 5005, Australia

(Received 2 May 2007; accepted 6 September 2007; published online 6 November 2007)

A fast and accurate numerical technique is developed for solving the biharmonic equation in a multiply connected domain, in two dimensions. We apply the technique to the computation of slow viscous flow (Stokes flow) driven by multiple stirring rods. Previously, the technique has been restricted to stirring rods of circular cross section; we show here how the prior method fails for noncircular rods and how it may be adapted to accommodate general rod cross sections, provided only that for each there exists a conformal mapping to a circle. Corresponding simulations of the flow are described, and their stirring properties and energy requirements are discussed briefly. In particular the method allows an accurate calculation of the flow when flat paddles are used to stir a fluid chaotically. © *2007 American Institute of Physics*. [DOI: 10.1063/1.2789970]

I. INTRODUCTION

In this paper we investigate a two-dimensional model for a highly viscous Newtonian fluid, stirred in a vat by the motion of one or more stirring rods: a "batch stirring device" (or BSD).[1] As one might expect from everyday experience, a fluid can readily be stirred effectively in such a device,[1–5] even in the Stokes flow regime, as examined here. The key to effective operation of the BSD is that it should generate *chaotic advection*,[6,7] in which the Lagrangian paths of fluid particles are chaotic. A particularly attractive feature of the BSD, as noted by Boyland, Aref, and Stremler,[1] is that it allows one to use a multiplicity of stirring rods. Then if these rods are made to undergo topologically nontrivial motions, it is possible to build-in certain desirable stirring characteristics to the resulting motion.

However, reliable simulation of the motion of fluid particles in the BSD necessitates a knowledge of the corresponding velocity field to high accuracy. This poses a particular numerical challenge, even though the governing equation is simply the (linear) biharmonic equation $\nabla^4\psi=0$ for the stream function ψ, because the flow domain geometry is complicated and time dependent. It is perhaps not surprising then that, so far, numerical investigations of the BSD have simplified the geometry by employing stirring rods of circular cross section and (apart from the work of Vikhansky[5]) a vat that is itself also of circular cross section.

For a circular cross section of both vat and rods, an exact expression for ψ is available when there is only one stirring rod,[3] but for more than one stirring rod no such exact expression is known, and it is necessary to compute the velocity field numerically. The computation may be carried out in a particularly accurate and efficient manner using complex-variable techniques:[4,8] the stream function is posed as the sum of appropriate singularities, together with corrections in the form of complex power series. The coefficients in these series decay rapidly, and so only a small number of terms need be kept to provide an extremely accurate numerical expression for the velocity field. The method is far superior, both in terms of accuracy and efficiency, than comparable finite-difference techniques, for instance. Furthermore, numerical solutions based on this technique agree well with careful laboratory experiments[8] with two circular stirring rods (see also Refs. 2 and 3).

However, the choice of a circular cross section for the stirring rods is a default, driven by its simplicity rather than any inherent practical desirability. In preference, one might choose the cross-sectional profile of a paddle, or an impeller. Unfortunately, the complex-variable numerical technique of Refs. 4 and 8 drastically worsens in performance if it is applied naively to noncircular rod cross sections. So in this paper we show how the technique can be modified to accommodate stirring rods of general cross section, provided only that the cross section of each rod may be mapped conformally to a circle; as particular cases, we describe elliptical rods and flat paddles.

The paper is arranged as follows: In Sec. II, we introduce the complex-variable formulation of the mathematical problem for Stokes flow in the BSD. We illustrate the numerical difficulties inherent in applying the solution technique of Refs. 4 and 8 directly to the problem with noncircular rod cross sections, and demonstrate a resolution. The instantaneous streamlines generated by various paddle motions are shown in Sec. III. These indicate how an increase in the eccentricity of the stirring rods, from circular to flat, progressively influences the flow field. In Sec. IV, we describe some numerical particle advection experiments, to show how "dyed" fluid is stirred by the BSD in various modes of operation. Our conclusions are given in Sec. V.

[a)]Electronic mail: stephen.cox@nottingham.ac.uk
[b)]Electronic mail: matthew.finn@adelaide.edu.au

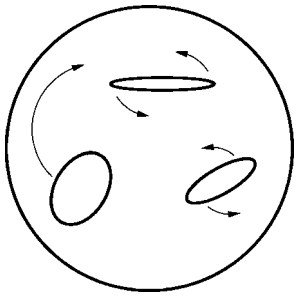

FIG. 1. A batch stirring device (BSD): viscous, incompressible fluid occupies the multiply connected region between the circular vat $|z|=a$, where $z=x+iy$, and m stirring rods (here drawn with elliptical cross section, for $m=3$). The arrows illustrate how the stirring rods may rotate about their axes and translate, in order to stir the fluid.

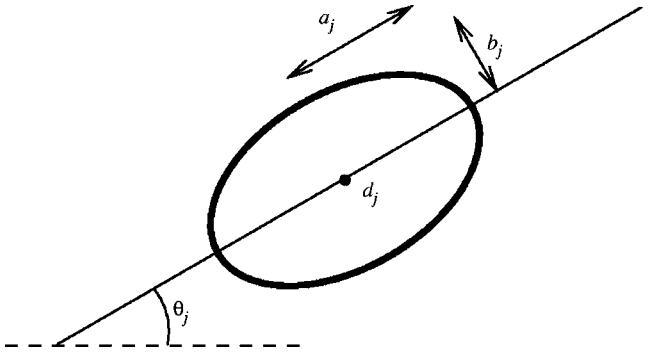

FIG. 2. Parameters of the jth elliptical stirring rod.

II. MATHEMATICAL FORMULATION

We suppose for definiteness that a highly viscous, incompressible fluid undergoes two-dimensional motion in a circular cylindrical vat whose wall is given by $|z|=a$, where $z=x+\mathrm{i}y$ (see Fig. 1). Inside the vat are m stirring rods, not necessarily of circular cross section. Let $z=d_j(t)$ be the center of the jth stirring rod $(j=1,\ldots,m)$; for a noncircular cross section, $d_j(t)$ might denote the centroid, for example. Denote the boundary of this rod by $\mathcal{B}_j$. Suppose that the jth stirring rod translates with velocity (U_j,V_j) and rotates about the point $z=d_j$ with angular velocity Ω_j. Then the no-slip boundary condition may be stated as

$$u+iv=U_j+iV_j+i\Omega_j(z-d_j) \quad \text{on } \mathcal{B}_j \ (j=1,\ldots,m) \tag{1}$$

and

$$u+iv=0 \quad \text{on } |z|=a, \tag{2}$$

where (u,v) is the fluid velocity.

For Stokes flow, the stream function ψ, in terms of which $(u,v)=(\psi_y,-\psi_x)$, satisfies the biharmonic equation[9]

$$\nabla^4\psi=0. \tag{3}$$

In this complex-variable formulation, the general solution to Eq. (3) may be written as

$$\psi(z,\bar{z};t)=\Re\{\bar{z}f(z;t)+g(z;t)\}, \tag{4}$$

for some functions f and g, which are analytic functions of z, and where $\Re$ denotes the real part of its argument. Because the fluid responds instantaneously to the boundary forcing, time may be considered to be a parameter characterizing the instantaneous configuration of the BSD when determining the functions f and g. The problem is to determine f and g consistent with the boundary conditions (1) and (2). Once ψ is known, the velocity components may readily be derived from Eq. (4) using

$$u+iv=-2i\frac{\partial\psi}{\partial\bar{z}}; \tag{5}$$

the vorticity ω and pressure p follow from[10]

$$p-i\mu\omega=8\mu i f'(z;t), \tag{6}$$

where μ is the coefficient of viscosity of the fluid, and where the prime denotes a z-derivative.

In what follows, we focus particularly on stirring rods of elliptical cross section, although the numerical technique developed below is by no means limited in this way. We denote the major and minor semiaxes of the jth elliptical stirring rod by a_j and b_j, respectively, with the major axis orientated at an angle $\theta_j(t)$ to the real axis (see Fig. 2). We shall later require a map from the boundary of this rod to the unit circle

$$w=\exp i\phi, \quad 0\leqslant\phi<2\pi, \tag{7}$$

which is achieved by the Joukowski transformation[10]

$$z=d_j+\tfrac{1}{2}l_j(w+c_j^2w^{-1})e^{i\theta_j}, \tag{8}$$

where

$$l_j=a_j+b_j \quad \text{and } c_j=\sqrt{\frac{a_j-b_j}{a_j+b_j}}.$$

It is important to note that we consider Eq. (8) to be a mapping between the region *outside* the circle in the w plane described by Eq. (7) and the region *outside* the jth ellipse in the z plane described by Eqs. (7) and (8) together. This specification of the domain and range of Eq. (8) is of particular importance when Eq. (8) is inverted to obtain $w=w(z;t)$, since in general Eq. (8) has two solutions for w given any point z outside the jth ellipse. The solution of relevance is the one with $|w(z;t)|>1$.

There are two special cases worthy of note. The first is the circular cross section, for which $a_j=b_j$, where the angle θ_j is irrelevant [and may therefore be taken in Eq. (8) to be zero]; here the map (8) becomes simply $z=d_j+a_jw$. The second is the flat plate of length $2a_j$ (i.e., with $b_j=0$), for which $z=d_j+a_j(w+w^{-1})e^{i\theta_j}/2$.

Method of solution

To determine ψ, we begin with Eq. (4), so that the governing biharmonic equation is satisfied identically. We then pose particular forms for f and g, and determine the associated coefficients by minimizing the residual error in the boundary conditions.

One motivation for the form of ψ posed below is the exact expression available in the case of a single stirring rod of circular cross section, i.e., for $m=1$ and $a_1=b_1$.[3] There, ψ is comprised of a Stokeslet and rotlet singularity inside the stirring rod, together with their image singularities in the vat wall, with the appropriate locations of the singularities being determined by geometrical considerations. If one did not have such an exact solution on hand, then a highly accurate numerical solution for ψ could be determined by writing ψ as the sum of Stokeslet and rotlet singularities at the *center* of the stirring rod, together with a compensating series in inverse powers of $z-d_1$. The strengths of the singularities and the coefficients in the series could then readily be determined by minimizing the mean squared error in the boundary conditions, evaluated at a large number of boundary points. This series solution proves to converge rapidly, and with only 20 or so terms can provide a numerical solution as accurate as that obtained from the exact formula for ψ; the basis for the high accuracy is the spectral convergence of a Fourier series for an infinitely differentiable periodic function (such as the prescribed boundary conditions).

For $m>1$ circular stirring rods, the stream function may efficiently be written similarly as the sum of Stokeslet and rotlet singularities, one of each type located at the center of each stirring rod, together with series in inverse powers of $z-d_j$ for each $j=1,\ldots,m$.[4,8] The singularity strengths and the coefficients in the various series are again computed numerically by minimizing the residual error in the boundary conditions, and the series again prove to be rapidly convergent. One is thus able to compute the velocity field to high accuracy and hence carry out reliable numerical dye-advection experiments, to evaluate the stirring properties of the resulting flows.

It is worthwhile now considering rather more precisely how an appropriate form for ψ may be derived from the specification of the problem above. Since the pressure and vorticity must be single-valued, it follows from Eq. (6) that $f'(z;t)$ is a single-valued function of z. Thus (if we suppress the time-dependence of the coefficients), $f'(z;t)$ may be written in the form

$$f'(z;t)=\sum_{k=0}^{\infty}F_k z^k+\sum_{j=1}^{m}\sum_{k=1}^{\infty}\frac{F_{j,k}}{(z-d_j)^k}.$$

This form represents $f'(z;t)$ as comprising a Taylor series about the origin *and* separate Laurent series about *each* of the rod centers, and gives the most general permissible form for $f'(z;t)$. Integration with respect to z then gives $f(z;t)$ in the form

$$f(z;t)=\sum_{k=0}^{\infty}\frac{F_k z^{k+1}}{k+1}-\sum_{j=1}^{m}\sum_{k=2}^{\infty}\frac{F_{j,k}}{(k-1)(z-d_j)^{(k-1)}}+\sum_{j=1}^{m}F_{j,k}\log(z-d_j). \tag{9}$$

Since the velocity field must also be single-valued, it follows from Eqs. (4) and (5) that the quantity $f(z;t)+z\bar{f}'(\bar{z};t)+\bar{g}'(\bar{z};t)$ is a single-valued function of position. But $f'(z;t)$ has already been forced to be single-valued, so it follows that $f(z;t)+\bar{g}'(\bar{z};t)$ is single-valued, and hence that $g'(z;t)$ may be written in the form

$$g'(z;t)=\sum_{k=0}^{\infty}G_k z^k+\sum_{j=1}^{m}\sum_{k=1}^{\infty}\frac{G_{j,k}}{(z-d_j)^k}+\sum_{j=1}^{m}\bar{F}_{j,k}\log(z-d_j);$$

the logarithm terms in $g'(z;t)$ are chosen so that $f(z;t)+\bar{g}'(\bar{z};t)$ contains logarithms of the form $F_{j,k}\log|z-d_j|^2$, which is single-valued. Then upon integration we find

$$g(z;t)=\sum_{k=0}^{\infty}\frac{G_k z^{k+1}}{k+1}-\sum_{j=1}^{m}\sum_{k=2}^{\infty}\frac{G_{j,k}}{(k-1)(z-d_j)^{(k-1)}}+\sum_{j=1}^{m}G_{j,k}\log(z-d_j)+\sum_{j=1}^{m}\bar{F}_{j,k}(z-d_j)[\log(z-d_j)-1]. \tag{10}$$

The nature of the logarithmic terms that arise in the stream function ψ now deserve special consideration. We see from Eqs. (4), (9), and (10) that the "$z\log z$" terms in ψ arising from the jth stirrer take the form $F_{j,k}\bar{z}\log|z-d_j|^2$ and its complex conjugate. The corresponding "$\log z$" terms in ψ arise from two sources in Eq. (10), and take the form

$$H_j\log(z-d_j)+\bar{H}_j\log(\bar{z}-\bar{d}_j). \tag{11}$$

However, this expression is more general than permitted by the full problem, as we see by considering the flux of fluid through the jth boundary. Since the boundaries are all impermeable, this flux must be zero. But the flux is simply $[\psi]_j$, i.e., the change in ψ upon traversing the boundary counterclockwise. From Eq. (11), $[\psi]_j=2\pi i H_j-2\pi i\bar{H}_j$. Since this quantity must be zero, it follows that H_j is real-valued, and hence that the jth "$\log z$" contribution to ψ may be written in the form,

$$H_j\log|z-d_j|^2.$$

In light of the discussion above, we are now able to write down an appropriate form for the stream function for the problem of stirring by *circular stirring rods*, using Eqs. (9) and (10). However, if one applies the same series solution when the stirring rods are noncircular, the rapid convergence is dramatically lost, as we shall illustrate below, because a series in $z-d_j$ no longer corresponds to a Fourier series when evaluated on the jth rod. In particular, it becomes infeasible to compute the stream function for elliptical paddles of even moderate eccentricity, for example. Fortunately the rapid

convergence can be recovered by a straightforward modification to the form of the series solution, which involves conformally mapping each boundary to the unit circle (L. N. Trefethen, personal communication). Specifically, if w lies on the unit circle, as in Eq. (7), and if $w=w_j(z)$ provides a conformal mapping that takes $z\in\mathcal{B}_j$ to the unit circle, and maps the region *outside* one boundary to that *outside* the other, then the sums in the ansatz for ψ should simply be written in terms of the $w_j(z)$ rather than $z-d_j$. The key point is that sums in powers of $w_j(z)$ *do* correspond to spectrally convergent Fourier series.

It should be emphasized that the method does not involve applying a single conformal mapping from the entire flow domain to some simpler region of the complex plane; this would be an exceedingly difficult task, and the mapping would change at each time step. Rather, the use of conformal mappings is purely a device to improve the numerical convergence properties of the various series.

In solving the present problem with circular stirring rods,[4] we previously used a "circle theorem" for the biharmonic equations[11,12] to modify the form of ψ to ensure that the no-slip boundary condition on the vat wall is satisfied automatically; essentially the modification involves appending to ψ appropriate images in this wall. However, the use of the circle theorem, while mathematically elegant, adds considerably to the algebraic complexity of ψ, and here we adopt instead the simpler device of including in ψ an additional series in positive powers of z [cf. Eqs. (9) and (10)], whose coefficients are determined in the process of minimizing the error in the boundary conditions. (We note that *inverse* powers of z are inappropriate, since the origin will often lie in the flow domain and a singularity is inappropriate there.) The boundary conditions on $|z|=a$ are then imposed numerically in the same way as on the stirring rods, as described below.

We are finally in a position to write down the stream function, in the form

$$\psi=\Re\sum_{j=1}^{m}(p_{j,1}\bar{z}+q_{j,1})\log|w_j(z)|+\Re\sum_{j=1}^{m+1}\sum_{k=2}^{n}(p_{j,k}\bar{z}+q_{j,k})w_j^{1-k}(z),\tag{12}$$

where the terms for $j=1,\ldots,m$ correspond to the respective stirring rods, and $j=m+1$ corresponds to the vat wall. In Eq. (12), we have introduced the notational trick of writing $w_{m+1}(z)=1/z$; thus the terms for $j=m+1$ provide a series in positive powers of z, leading to spectral convergence for the vat wall boundary condition (2). The series are truncated at $k=n$ to provide our numerical approximation (cf. Refs. 4 and 8). The Stokeslet and rotlet singularities mentioned above correspond, respectively, to the terms with coefficients $p_{j,1}$ and $q_{j,1}$. With ψ given by the ansatz (12), all physical quantities (velocity, vorticity, and pressure) are single-valued, provided Eq. (8) is inverted appropriately to find $w(z)$. In particular, the fluid velocity is from Eq. (5),

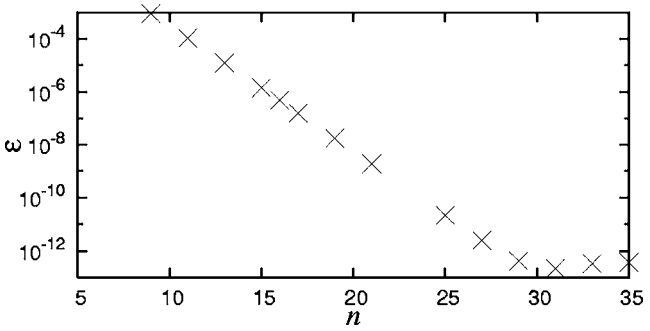

FIG. 3. Maximum absolute error ϵ in the boundary velocity for a single circular paddle ($a_1=b_1=0.3$) centered at $z=0.5+0i$ and rotating about its axis ($\Omega_1=1$, $U_1=V_1=0$), plotted against the number of terms n taken in Eq. (8). Note the exponential decay of ϵ with n, until limits of machine precision are reached.

$$u+iv=-i\sum_{j=1}^{m}\left\{p_{j,1}\log|w_j(z)|+\frac{1}{2}(p_{j,1}\bar{z}+q_{j,1}+\bar{p}_{j,1}z+\bar{q}_{j,1})\frac{\bar{w}_j'(\bar{z})}{\bar{w}_j(\bar{z})}\right\}-i\sum_{j=1}^{m+1}\sum_{k=2}^{n}\left\{p_{j,k}w_j^{1-k}(z)+(\bar{p}_{j,k}z+\bar{q}_{j,k})(1-k)\frac{\bar{w}_j'(\bar{z})}{\bar{w}_j^{k}(\bar{z})}\right\}.\tag{13}$$

To compute appropriate values for the coefficients in Eq. (12), we minimize (numerically) the residual squared error in the boundary conditions, computed at a large number of points. Specifically, around each boundary (i.e., around each stirring rod and around the vat wall) we place $N\equiv 5n$ points; around the vat wall, the relevant points are equispaced, while for the jth stirring rod, these points are equally spaced in ϕ around $w_j(\phi)=\exp i\phi$ (this generally clusters points around the more highly curved ends of the rods). The redundancy factor $N/n=5$ is the result of some trial and error, and has no other particular significance. We let $\boldsymbol{r}$ be a vector comprising the real and imaginary parts of all the unknown coefficients in Eq. (12), and $\boldsymbol{\chi}$ be a vector of expressions for the values of u and v at all the $(m+1)N$ sample points on the various boundaries, obtained from Eq. (13). The desired boundary values of the velocity components at the corresponding points are then collected in a vector $\boldsymbol{\Phi}$. Denoting by M the matrix with elements $M_{ij}=\partial\chi_i/\partial r_j$, we see that the boundary conditions (1) and (2) amount to the matrix equation $M\boldsymbol{r}=\boldsymbol{\Phi}$. A least-squares solution is found by first computing the singular value decomposition of $M\equiv\mathcal{U}\mathcal{S}\mathcal{V}^T$, where $\mathcal{S}$ is the diagonal matrix of the singular values $\{s_j\}$. The least squares choice of parameters is then given by $\boldsymbol{r}=\mathcal{V}\mathcal{S}^*\mathcal{U}^T\boldsymbol{\Phi}$, where the elements of the diagonal matrix $\mathcal{S}^*$ are $\{s_j^{-1}\}$, except where s_j is less than some numerical tolerance, in which case the corresponding element of $\mathcal{S}^*$ is set to zero. The whole procedure is accomplished easily in MATLAB (see the Appendix), with the least-squares calculation performed using the matrix pseudoinverse $r=\text{pinv}(M)*\text{Phi}$.

Figure 3 shows the maximum absolute error ϵ in the computed boundary velocities for a flow generated by a

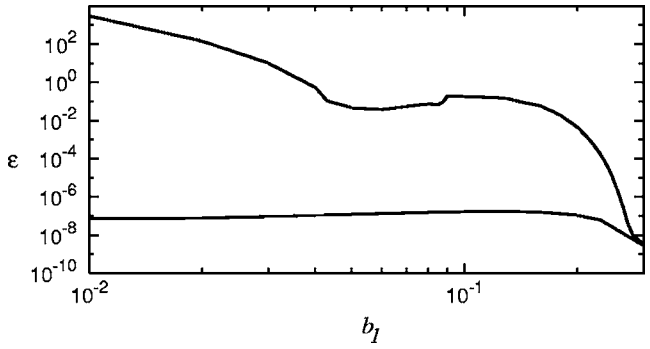

FIG. 4. Maximum absolute error ϵ in the boundary velocity for a single elliptical paddle with $a_1=0.3$, centered at $z=0.5+0i$ and moving with unit speed parallel to the x-axis ($U_1=1$, $V_1=\Omega_1=0$), for $n=21$ and a range of values of b_1. Comparison between solution expressed in terms of w_1 (lower curve) or in terms of $z_1=2(z-d_1)/l_1$ (upper curve), see text. Note the huge errors in a naive application of the prior method (upper curve) and the dramatic advantage of the present formulation (8), even for moderate eccentricity of the stirring rod.

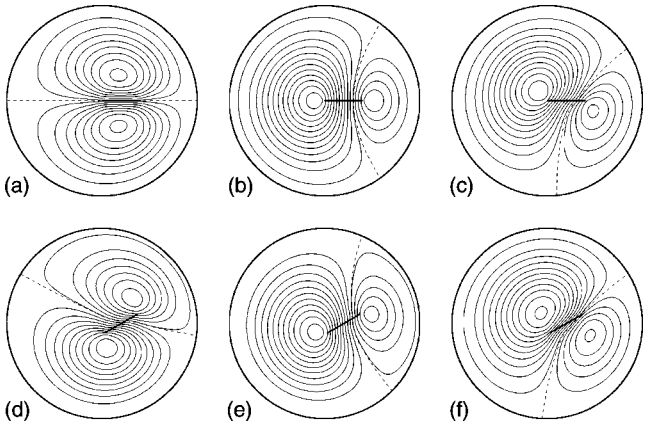

FIG. 5. Streamlines for a paddle of length 0.4, centered $z=0.2+0.0i$. Top row: $\theta_1=0$. Translation (a) in the x-direction, (b) in the y-direction, (c) at a 45° angle. Bottom row: $\theta_1=\pi/6$. Translation (d) in the x-direction, (e) in the y-direction, (f) at a 45° angle.

single stirring rod. The rod is circular, with $a_1=b_1=0.3$, and rotates with unit angular velocity about its axis, at $d_1=0.5+0i$. The error appears to decrease exponentially with increasing truncation parameter n, until the limits of machine precision are reached.

Figure 4 shows the effects upon ϵ of varying the eccentricity of an elliptical stirring rod, and demonstrates the necessity of the conformal mappings implicit in Eq. (12). Here the truncation parameter is fixed to be $n=21$ and the major semiaxis of the rod is $a_1=0.3$. The remarkable feature of this figure is the extremely poor performance (upper curve) obtained by naively adopting the formulation in Ref. 4 for the stream function, so that the series in Eq. (12) are written in powers of $2(z-d_j)/l_j$ rather than powers of w_j. That method is unusable for even modest departures from a circular cross section. The lower curve in Fig. 4 shows how the current method resolves the difficulty, and shows that in a proper formulation the residual numerical error is largely insensitive to the aspect ratio b_1/a_1 of the stirring rod cross section; indeed, we find similar results down to $b_1=10^{-7}$, and even in the limiting case of a perfectly flat paddle with $b_1=0$.

For various values of m (the number of stirring rods), and for various eccentricities of the stirring rods, we find that we are generally able to satisfy the boundary conditions essentially to within machine precision. This gives us some confidence that our expression (12) for the stream function does indeed provide sufficient generality.

III. STREAMLINES OF THE FLOW

In this section we illustrate some typical streamlines, for $m=1,2,3$; here, lengths are scaled so that the vat has a unit radius. These results provide some insight into the effects upon the flow of a noncircular cross section for the stirring elements.

There have been extensive previous studies of the streamline topology due to the motion of *circular* stirring rods in a device such as described here. We have elsewhere[3] given some typical streamline patterns for $m=1$. For $m=2$, Jana, Metcalfe, and Ottino[13] found a variety of possible topologies, even in the restricted problem that has a symmetrical configuration of stirring rods (but not necessarily symmetrical motions) and rotation of each rod about a fixed axis only (i.e., no translation). The catalog of streamline topologies in this case was extended by Price, Mullin, and Kobine.[8] All three of these papers involved a combined numerical and experimental investigation, and demonstrated excellent agreement between the two approaches. An exploration of the possibilities for $m=3$ was begun by Hajjam.[14] The results presented below, for one, two, and three elliptical paddles, are intended to be illustrative of the sorts of streamline patterns that might be found in "reasonable" configurations of a BSD; they are clearly far from comprehensive. We note that the parameter space to be explored for elliptical paddles is significantly larger than that for circular paddles due to the nontrivial effects of orientation and aspect ratio in the former case.

Because the previous work highlighted above has focused exclusively on the case of circular stirring rods, we focus here on properly elliptical paddles, and primarily on the (admittedly rather arbitrary) case with aspect ratio $b_j/a_j=10^{-3}$. We shall refer in our discussion below to such paddles as flat, and to $2a_j$ as the length of the paddle (although one might argue that the term "length" strictly makes sense only if $b_j=0$). Each of our plots of the stream function ψ shows contours in equal increments; to some extent this allows "differentiation by eye" to estimate the velocity field, although it does mean that some of the weaker (and therefore less significant) eddies may not be visible in the plots that are presented here. Also shown, as dashed lines, are separatrices of the flow.

Figure 5 shows streamlines generated by translation of a single flat paddle, of length 0.4 (i.e., with $a_1=0.2$), instantaneously centered at $z=0.2+0.0i$. In each case, two eddies are formed, one clockwise and one counterclockwise. For the case $\theta_1=0$ (first row of the figure), so that the flow domain has symmetry about the x-axis, the streamlines generated by the paddle resemble those due to a circular stirring rod: motion parallel to either the x- or y-axis generates streamlines with symmetry about the x-axis; motion at a 45° angle, for

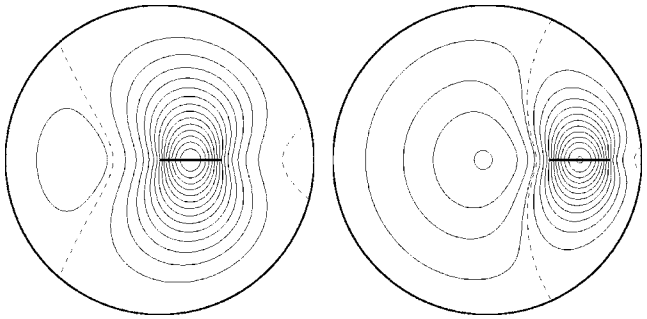

FIG. 6. Streamlines for a paddle of length 0.4, with $\theta_1=0$, rotating about its axis. Left: centered at $z=0.2+0.0i$. Right: centered at $z=0.6+0.0i$.

instance, breaks this symmetry. Of course, as the second row of the figure shows, with a different orientation of the flat paddle, the streamlines are no longer symmetrical in the x-axis even when the paddle motion is parallel to one of the axes.

Figure 6 shows streamlines generated by a paddle rotating about its axis, when placed at two different locations on the diameter of the vat. In each case there are three eddies, one in the same sense as the paddle, and two others, away from the paddle, in the opposite sense. The smallest eddy is very weak; we have verified its existence by plotting streamlines in higher resolution (not shown here). This behavior is in contrast to that of a circular stirring rod, where a rod placed near the center of the vat seems to generate a single eddy, while a sufficiently off-center rod generates two (cf. Ref. 3).

Figure 7 shows the evolution of the instantaneous streamlines as a paddle rotates about its axis, at a fixed location. There appear to be three eddies in the streamline plot at any instant. This flow differs significantly from the corresponding (steady) flow due to a circular rod; here the geometry of the device is time-dependent, hence the flow is time-dependent. This simple observation has profound consequences for the motion of the fluid: with a circular rod, all particle paths are time-periodic; with a paddle, some may be chaotic, thereby greatly enhancing mixing.

Figure 8 shows two paddles, whose centers lie on a diameter of the vat, one stationary and the other rotating about its axis. At any instant one can identify three eddies; however, their topology varies significantly with time. For example, the main, central eddy sometimes encloses only the right paddle, and sometimes encloses both. We see from the central panel of Fig. 8 a mechanism by which fluid near the

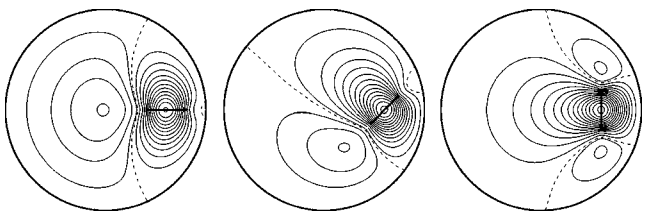

FIG. 7. Streamlines for a paddle of length 0.4, centered at $z=0.6+0.0i$, rotating about its axis. From left to right: $\theta_1=0$, $\pi/4$, $\pi/2$.

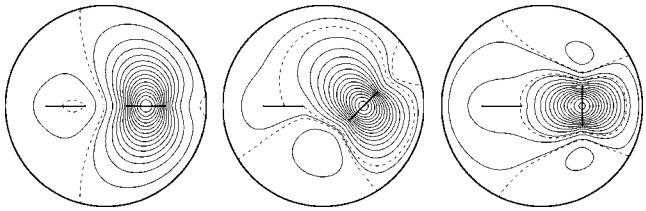

FIG. 8. Streamlines for two paddles, each of length 0.4, centered at $z=\pm 0.4+0.0$i. The left paddle is stationary while the right paddle rotates about its axis. In each case, $\theta_1=0$ for the left paddle. For the right paddle, from left to right: $\theta_1=0$, $\pi/4$, $\pi/2$.

left paddle can mix with the bulk. A further feature of note is that small recirculation zones appear intermittently on the stationary paddle.

Figure 9 shows the streamlines generated by two paddles, each rotating about its axis with the same angular speed, but in opposite senses. If the paddles are both initially aligned with the vat diameter on which their centers lie, say, then a symmetry of the streamlines about the orthogonal diameter is maintained during operation of the device, causing a significant barrier to mixing, since fluid particles are not advected between left and right halves of the device (see left and center panels of the figure). At different instants in the motion of the paddles, there may be two eddies (left panel), or up to six (center panel). If the initial orientations of the paddles are chosen instead so that they are never simultaneously in alignment with their common diameter (right panel), then the left-right symmetry of the flow is broken, thus removing a significant impediment to mixing of the fluid between the two sides.

Figure 10 shows the streamlines for two paddles rotating in the same sense. We have chosen the orientations of the paddles so that they are exactly in-phase. In the left and center panels, $\theta_j=0$ for each paddle at the instant shown, and there are five eddies. The right panel illustrates the streamlines later in the motion of the device ($\theta_j=\pi/2$ for $j=1,2$), with six eddies.

In the next section we shall describe simulations of stirring by a three-paddle device, and so we illustrate in Fig. 11 some streamlines for this case. The paddles are initially centered at $z=0$ and at $z=\pm 4/7+0i$ and each have a length of $2/7$; the leftmost paddle is stationary while the other two rotate about the point $z=2/7+0i$. Finally, we compare in this figure the streamlines generated by paddles with those for circular stirring rods. Although the streamlines are little dif-

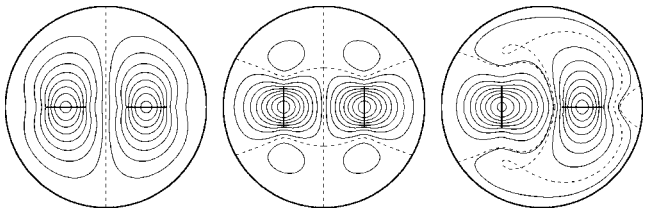

FIG. 9. Streamlines for two paddles, each of length 0.4, centered at $z=\pm 0.4+0.0i$, rotating with equal but opposite angular velocities. Left: $\theta_j=0$ for both paddles. Center: $\theta_j=\pi/2$ for both paddles. Right: $\theta_1=\pi/2$, $\theta_2=0$.

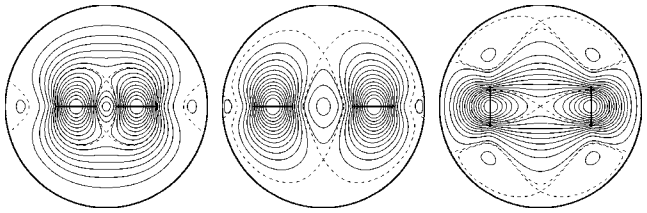

FIG. 10. Streamlines for two paddles, each of length 0.4. The paddles rotate with equal angular velocities, in the same sense. Left: paddles centered at $z=\pm 0.3+0.0i$, $\theta_j=0$ $(j=1,2)$. Center: paddles centered at $z=\pm 0.5+0.0i$, $\theta=0$ $(j=1,2)$. Right: paddles centered at $z=\pm 0.5+0.0i$, $\theta=\pi/2$ $(j=1,2)$.

ferent in the two cases, some differences emerge when we calculate the power input required to drive the device in the two cases. For the situation shown in the last two panels of Fig. 11, with the rightmost stirring rods rotating with angular velocity Ω about the point $z=2/7+0i$, the power input per unit area (and per unit length in the third coordinate direction) is $k\mu\Omega^2$, where $k=1.725$ (paddles) or $k=2.131$ (circles). Correspondingly, for stirring rods instantaneously lying along a common diameter, with the rightmost pair again rotating about the point $z=2/7+0i$ with angular velocity Ω (cf. first panel of the figure), the requisite power inputs have $k=1.603$ (paddles) and $k=1.932$ (circles). In each configuration the power input required for the paddles is almost 20% less than for the circular stirring rods.

IV. NUMERICAL SIMULATIONS OF STIRRING

We describe in this section numerical simulations of stirring by circular rods and elliptical paddles. In each case, passive "dyed" tracer particles are simulated—these move with the flow but do not influence it. We employ two diagnostics of the stirring. The first, the iterated mapping plot,[6] gives qualitative information about the long-time behavior of fluid particles, and indicates regions of regular and chaotic Lagrangian particle paths. Although its relevance to short-time mixing may be disputed,[13] the iterated mapping does provide a strong visual indication of the extent, if any, of the chaotic regions. The second diagnostic is the rate of stretch of a finite material line. This diagnostic is computationally expensive if we maintain adequate resolution of the exponentially growing line. In our calculations we dynamically insert particles into the initial line so as to maintain an acceptable tolerance between neighboring particles in the stretched line (cf. Ref. 15). Then, at least at modest computational expense, it is feasible to track the line only for a few periods of the flow.

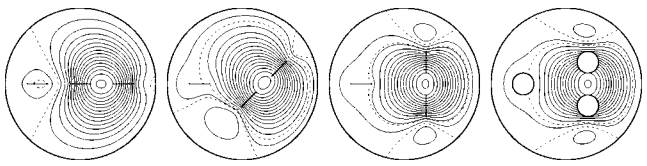

FIG. 11. First three plots: streamlines for three paddles, each of length 2/7. The leftmost paddle is stationary while the other two rotate about a point midway between their centers. Right: corresponding flow generated by circular stirring rods, of diameter 2/7.

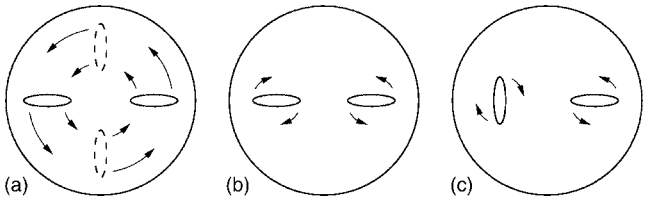

FIG. 12. (a) Simple mixer with two paddles generates only regular motion because transformation to a rotating frame results in a time-independent problem. (b) Dual-impeller mixer, shown for counter-rotating paddles; this initial condition yields a flow symmetrical under reflection in the y-axis if the angular velocities of the impellers are equal and opposite. (c) Dual-impeller mixer with this symmetry broken by "staggering" the orientation of the paddles.

A. Two paddles

With two paddles, an easily constructed mixer is as follows [see Fig. 12(a)]: two paddles are placed with their centers on some diameter of the vat, with their major axes pointing along this diameter. The diameter in question then rotates. However, this design fails to generate chaotic particle paths; only regular fluid particle motions are generated, because in a frame of reference rotating appropriately about the vat center with the paddles the flow is steady.

Figures 12(b) and 12(c) show two variants of a simple "dual-impeller" design that *does* generate chaos. In each case the left paddle rotates clockwise and the right paddle counterclockwise, with equal angular speeds. However, if the device maintains symmetry about the y-axis during operation, for example by starting both paddles horizontally or vertically, then there are many small (but visible) regular regions in the chaotic sea [see Fig. 13(a)]. Far better is to "stagger" the paddles, as in Fig. 12(c). Figure 13(b) shows the corresponding dramatic improvement if the major axes of the paddles are orthogonal, rather than parallel, at the start of their motion.

For the configuration in Fig. 13(b), we show in Fig. 14 that the aspect ratios of the paddles need not be far from unity to generate a significant chaotic region. (Recall that for circular stirring rods the flow is steady and all trajectories are regular.) The size of the regular regions around the paddles evidently decreases as the paddles become less circular. In all

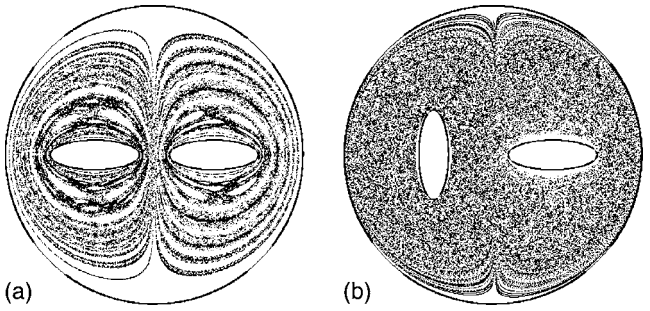

FIG. 13. Iterated mapping plots for two paddles, corresponding to Figs. 12(b) and 12(c). In each case the paddles are centered at $\pm 0.4+0i$; $a_j=0.3$, and $b_j=0.1$ (for $j=1,2$). (a) $\theta_1=-2\pi t$ and $\theta_2=2\pi t$, for left and right paddles, respectively. (b) $\theta_1=2\pi(1/4-t)$ and $\theta_2=2\pi t$.

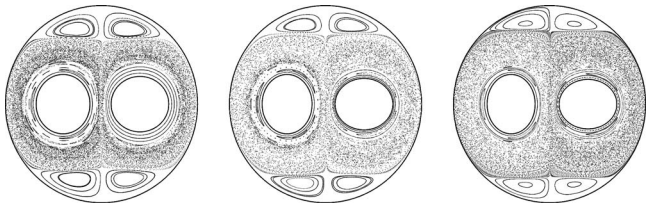

FIG. 14. Iterated mapping plots for two paddles. In each case the paddles are centered at $\pm 0.4+0i$ with $a_j=0.3$ (for $j=1,2$). Furthermore, in each case $\theta_1=2\pi(1/4-t)$ and $\theta_2=2\pi t$ for left and right paddles, respectively (cf. Fig. 12), so there is no symmetry of the plot in the y-axis. From left to right: $b_j=0.28$, 0.26, 0.25 (for $j=1,2$). We see here the dramatic effects of even moderate eccentricity of the paddles; by contrast, circular stirring rods give rise to entirely integrable flows, with no chaotic regions.

three cases shown in Fig. 14, there are significant regular recirculation regions for relatively large $|y|$, in contrast to the more eccentric paddles of Fig. 13(b).

B. Topological chaos with three stirring elements

With one or two stirring elements, effective stirring generally requires tuning of the parameters of the system, for example, by varying the paths of the stirring elements, their sizes, and aspect ratios, or their rates of rotation about their respective axes. But a recent reinvigoration of the field has followed from the observation by Boyland, Aref, and Stremler[1] that for $m>3$ one can *build in* so-called "topological chaos" by using appropriate paddle motions that correspond to a nontrivial mathematical braid; this presents an appealing prospect for mixer designs that are robust to changes in operational parameters or fluid properties.

With $m=3$, we now describe two simple stirring protocols, each of which is generated by successively interchanging the positions of neighboring stirring rods. The only difference between the two protocols lies in whether all interchanges are carried out clockwise, or whether they are alternately clockwise and counterclockwise. It is useful to denote these interchanges by the symbols $L^{\pm}$ and $R^{\pm}$. In L^{-}, the rightmost paddle remains stationary, while the leftmost and center paddle are interchanged. The semicircular paths taken by the interchanging paddles are shown in Fig. 15. The superscript "$-$" indicates that the paddle centers rotate counterclockwise; a superscript "$+$" indicates clockwise motion. The interchanges $R^{\pm}$ likewise correspond to the interchange of the rightmost and center paddles, with the leftmost paddle fixed. The protocol $R^{-}L^{+}$ (reading from left to right, so that first R^{-} then L^{+} is carried out) is known to produce good mixing, while $R^{-}L^{-}$ produces poor mixing.[1] Here, we consider only the good protocol, and examine the effects of changes to the shape of the paddles and the rates at which they rotate about their axes during the stirring. We scale time so that the protocol $R^{-}L^{+}$ takes one time unit, and again scale lengths so that the vat has unit radius.

Figure 16 shows the evolution of a material line initially lying between $2/7\pm i/2$ under the flow generated by three circular stirring rods moving under the protocol $R^{-}L^{+}$. The circles have radius $1/7$ and their centers lie initially at 0 and $\pm 4/7$. Note that during the protocol, as Fig. 15 suggests, the relevant stirring rods rotate about their axes as they interchange with one another. We name this "Protocol A." The line initially has length 1; its length after successive periods of the motion is given in Table I.

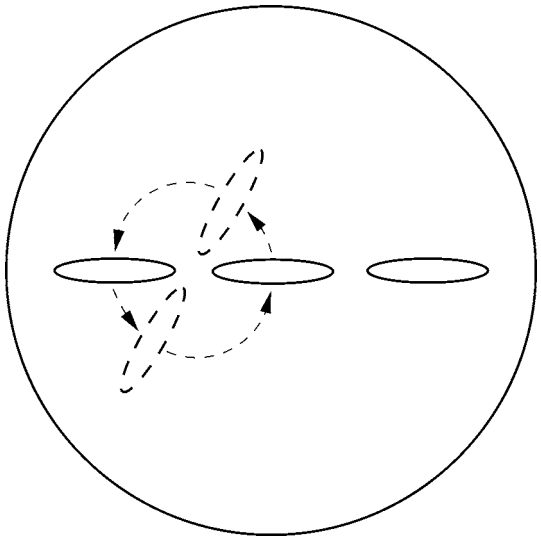

FIG. 15. Semicircular paths taken by paddles during the interchange L^{-}. All paddles begin and end the interchange with their centers on the real axis and with their major axes aligned along this axis. The rightmost paddle remains stationary. The leftmost paddle and center paddle interchange positions; they do so by rotating one half-revolution about the point midway between their centers.

If the circular rods are replaced by paddles with $a_j=1/7$ and $b_j=1/50$, we find the results shown in Fig. 17; we refer to this as "Protocol B." The kinks in the line are slightly more pronounced than in Protocol A, and consequently the rate of growth of the line is a little in excess of that for Protocol A.

If, during the interchanges, the paddles are made to rotate about their axes at twice the rate indicated in Fig. 15, one might expect some additional stretch of the line due the enhanced impeller motion. But in this case the line evolves as in Fig. 18 (Protocol C), and the additional rotation of the paddles seems to *reduce* some of the kinks seen in Fig. 17. Growth of the line is roughly as in Protocol A.

Finally, we consider the case in which the paddles do not rotate about their axes at all during the interchanges (Protocol D; see Fig. 19). Thus here their major axes always lie parallel to the x-axis. In terms of the line stretch after four periods, this protocol improves on the double rotation of Protocol C, but is worse than the "proper" rotation of Protocol B. The kinks observed in the line in Fig. 17 seem to be greatly reduced in this protocol.

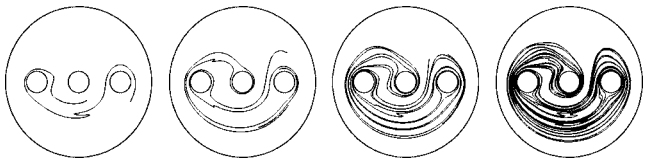

FIG. 16. Evolution of a line element, initially between $2/7\pm i/2$, with circular paddles, executing the protocol $R^{-}L^{+}$ (see text for further details). The stretched line is shown after 1, 2, 3, and 4 periods.

TABLE I. Length of line after 1–4 periods of the motion, for various protocols (see text for details). Initially the line lies between $2/7\pm i/2$, and so has unit length.

Protocol	1	2	3	4
A	4.25	13.1	36.5	95.3
B	4.27	14.2	42.1	123
C	4.00	12.9	34.8	95.3
D	3.84	11.9	37.5	108

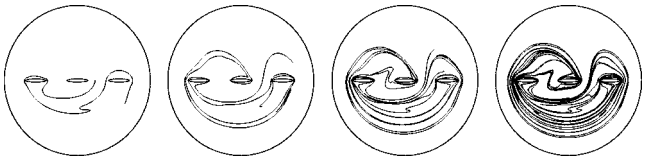

FIG. 18. Evolution of a line element, initially between $2/7\pm i/2$, with paddles having $a_j=1/7$, $b_j=1/50$ (for $j=1,2,3$), executing the protocol R^-L^+, as in Fig. 17, except that the paddles undergoing an interchange rotate about their axes at twice the rate there.

Since the initial location of the line is rather arbitrary, we might view its initial evolution as accidental, and measure the stretch rate of its interface only after its evolution appears to have settled down. To this end, if we use only the data after three and four periods to compute the factor by which the length of the line grows in the last period, we obtain for the four protocols *A*, *B*, *C*, and *D*, respectively, 2.61, 2.92, 2.73, and 2.88. These results confirm the ordering suggested by the values in the final column of Table I (but suggest that Protocol C is better than Protocol A).

In evaluating these protocols, we might ask how much energy is required for each. To specify the energy, we suppose for definiteness that the speed of the relevant paddle centers is the same during each interchange and use the result[3] that (in the dimensional problem) the energy input per period, per unit length in the third coordinate direction, is

$$\int_0^T 4\pi\mu\sum_{j=1}^{m}\{\Im(\bar{p}_{j,1}(U_j+iV_j))-(q_{j,1}+\Re(\bar{p}_{j,1}d_j))\Omega_j\}\mathrm{d}t,$$

where T is the (dimensional) period of the protocol. We find that this quantity takes the form $\mu a^2\mathcal{E}/T$, where a is the dimensional radius of the vat and for Protocols A, B, C, and D (respectively) $\mathcal{E}=141.3$, 121.3, 170.2, and 91.4. These results seem to recommend Protocol D.

V. CONCLUSIONS

The method described here permits accurate numerical solution of the biharmonic equation in a multiply connected domain, relevant to two-dimensional slow viscous flow generated by multiple stirring rods. We emphasize that the fluid motion satisfies boundary conditions appropriate to the no-slip condition on physical rods, and that, while expressions such as Eq. (12) involve singularities, none of these lie in the flow domain itself. The flow field is thus free of singularities, unlike models where the stirring rods are replaced by rotlets,[16] for example. This represents a significant advantage of the present case over singularity-driven flow, where the possible locations of the singularities are generally tightly constrained (and hence they must remain stationary, and "blink" on and off to generate a time-dependent flow).

The desire to simulate the trajectories of fluid particles in chaotic Stokes flows necessitates a particularly accurate solution for the velocity field. The methods described here provide at modest computational expense velocity fields which are in practice limited only by machine precision. Although it could be argued that expression (12) for the stream function ψ is mathematically inelegant, embodying as it does considerable redundancy in its large number of coefficients of multiple power series, it does provide a practical means of computing ψ with extreme accuracy. Furthermore, the conformal-mapping trick (suggested to us by L. N. Trefethen, personal communication) proves to be essential to recover rapid convergence of the various series in Eq. (12) and thereby to render the method useful for noncircular rod cross sections. We reiterate that the conformal mappings required are simply a device to improve the convergence of various series: their role is to map each rod cross section to a circle (leading to rapidly convergent Fourier series), and no *global* mapping is required from the complicated, time-dependent, multiply connected region to something simpler (cf. Ref. 17 for inviscid potential flow).

The ability to simulate the flow due to elliptical paddles (or, indeed, stirring elements with a wide variety of cross sections) allows the investigation of significantly better mixer designs than rods of circular cross section. This is because with circular stirring rods, the flow domain geometry is fixed if the centers of the rods are fixed in space and they drive the motion through (time-dependent) rotations

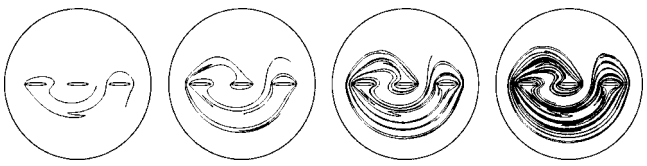

FIG. 17. Evolution of a line element, initially between $2/7\pm i/2$, with paddles having $a_j=1/7$, $b_j=1/50$ (for $j=1,2,3$), executing the protocol R^-L^+ (see text for further details). The stretched line is shown after 1, 2, 3, and 4 periods.

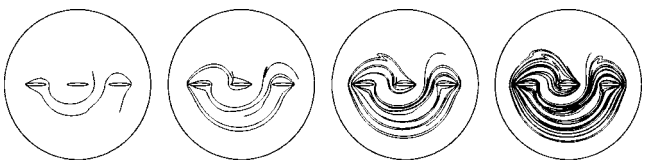

FIG. 19. Evolution of a line element, initially between $2/7\pm i/2$, with paddles having $a_j=1/7$, $b_j=1/50$ (for $j=1,2,3$), executing the protocol R^-L^+, as in Fig. 17, except that the paddles undergoing an interchange do not rotate about their axes.

about their respective axes, as has been a common setup in many prior Stokes flow studies. In the case of paddles, however, the geometry of the flow domain (and hence the flow itself) is necessarily time dependent. Our results indicate that even slight eccentricity of the paddles can lead to significant chaotic regions in the flow.

Finally, we note that series-solution techniques similar to those adopted here for Stokes flow may be used in solving Laplace's equation efficiently and accurately for inviscid potential flow in complicated, multiply connected geometries.

ACKNOWLEDGMENTS

We are grateful to a referee for suggesting significant improvements to our derivation and justification of the complex-variable methods used in this paper.

APPENDIX: MATLAB CODE

The calculations described in this paper are readily implemented in MATLAB, as illustrated below.

```
%SOL solve for coefficients in series solution.
% [P,Q]=SOL(N) returns P and Q that minimize the boundary error.

function [p,q]=sol(n)

global d a t o u;
% set collocation points and target velocities
m=length(d); N=5*n; s=exp(2*pi*i*linspace(0,1,N)).';
c=real(s)+1e-3*i*imag(s); z=s; Phi=zeros(size(s));
for j=1:m
    z=[z;d(j)+a(j)*c*exp(i*t(j))];
    Phi=[Phi;u(j)+i*o(j)*a(j)*c*exp(i*t(j))];
end
Phi=c2r(Phi);

% Build least squares matrix
r=zeros(4*(m+1),n);
M=zeros(length(Phi),length(r(:)));
for k=1:length(r(:))
    r(k)=1; V=c2r(vel(z,r2c(r(1:2*(m+1),:)),r2c(r(2*(m+1)+1:end,:))));
    M(:,k)=V(:).'; r(k)=0;
end

% solve by singular value decomposition method
r(:)=pinv(M)*Phi(:);
p=r2c(r(1:2*(m+1),:));
q=r2c(r(2*(m+1)+1:end,:));

% helpers to convert between real and complex matrices
function val=r2c(r)
[m,n]=size(r); h=m/2; val=r(1:h,:)+i*r(h+1:m,:);

function val=c2r(c)
val=[real(c);imag(c)];

%VEL compute velocity field.
% VEL(Z, P, Q) computes the velocity field at Z using coefficients P and Q

function u=vel(z,p,q)

[m,n]=size(p); u=zeros(size(z)); p(m,1)=0; q(m,1)=0;
zb=conj(z); pb=conj(p); qb=conj(q);

for j=1:m
  u=u-i*p(j,1)*log(abs(w(z,j))) ...
```

```
        -i/2*(p(j,1)*zb+q(j,1)+pb(j,1)*z+qb(j,1)).*conj(w(z,j,'d')./w(z,j));
  for k=2:n
    u=u-i*p(j,k)*w(z,j).^(1-k) ...
        -i*(pb(j,k)*z+qb(j,k))*(1-k).*conj(w(z,j,'d')./w(z,j).k);
  end
end

%W compute conformal mappings.
% W(Z,J,D) computes the conformal mapping of Z onto each W domain. If a
% flag is given the function returns the derivative of the map instead.

function q=w(z,j,der)

global d a t;
unity=1.0001; m=length(d);

if (nargin<3) % calculate mapping
  switch j
      case m+1
        q=1./z;
      otherwise
        z=exp(-i*t(j))/a(j)*(z-d(j));
        sgn=2*(real(z)>=0)-1;
        q=z+sgn.*sqrt(z.^2-unity);
  end
else % calculate derivative
  switch j
      case m+1
        q=-1./z.^2;
      otherwise
        z=exp(-i*t(j))/a(j)*(z-d(j));
        sgn=2*(real(z)>=0)-1;
        q=(1+sgn.*z./sqrt(z.^2-unity)).*exp(-i*t(j))/a(j);
  end
end

%PSI compute stream function.
% PSI((Z,P,Q)) computes the stream function at Z using coefficients P and Q.

function u=psi(z,p,q)

[m,n]=size(p); u=zeros(size(z)); p(m,1)=0; q(m,1)=0;
zb=conj(z); pb=conj(p); qb=conj(q);

for j=1:m
  u=u+real((p(j,1)*zb+q(j,1)).*log(abs(w(z,j))));
  for k=2:n
    u=u+real((p(j,k)*zb+q(j,k)).zbw(z,j).^(1-k));
  end
end

% demonstration that computes the streamlines on the right in Fig. 9.

global d a t o u;

d=[-0.4 0.4]; a=[0.2 0.2]; t=[pi/2 0]; o=[-1 1]; u=[0 0];

[x,y]=meshgrid(linspace(-1,1,100)); z=x+i*y;
[p,q]=sol(12); s=psi(z,p,q);
contour(x,y,s,linspace(-0.0583,0.0024,16));
```

[1] P. L. Boyland, H. Aref, and M. A. Stremler, "Topological fluid mechanics of stirring," J. Fluid Mech. **403**, 277 (2000).
[2] M. J. Clifford, S. M. Cox, and M. D. Finn, "Reynolds number effects in a simple planetary mixer," Chem. Eng. Sci. **59**, 3371 (2004).
[3] M. D. Finn and S. M. Cox, "Stokes flow in a mixer with changing geometry," J. Eng. Math. **41**, 75 (2001).
[4] M. D. Finn, S. M. Cox, and H. M. Byrne, "Topological chaos in inviscid and viscous mixers," J. Fluid Mech. **493**, 345 (2003).
[5] A. Vikhansky, "Simulation of topological chaos in laminar flows," Chaos **14**, 14 (2004).
[6] H. Aref, "Stirring by chaotic advection," J. Fluid Mech. **143**, 1 (1984).
[7] H. Aref, "The development of chaotic advection," Phys. Fluids **14**, 1315 (2002).
[8] T. J. Price, T. Mullin, and J. J. Kobine, "Numerical and experimental characterization of a family of two-roll-mill flows," Proc. R. Soc. London, Ser. A **459**, 117 (2003).
[9] H. Lamb, *Hydrodynamics*, 6th ed. (Cambridge University Press, Cambridge, 1932).
[10] L. M. Milne-Thomson, *Theoretical Hydrodynamics* (Macmillan, New York, 1968).
[11] A. Avudainayagam and B. Jothiram, "A circle theorem for plane Stokes flows," Q. J. Mech. Appl. Math. **41**, 383 (1988).
[12] S. K. Sen, "Circle theorems for steady Stokes flow," ZAMP **40**, 139 (1989).
[13] S. C. Jana, G. Metcalfe, and J. M. Ottino, "Experimental and computational studies of mixing in complex Stokes flows: The vortex mixing flow and multicellular cavity flows," J. Fluid Mech. **269**, 199 (1994).
[14] M. Hajjam, "Comportement des lignes de décollement en régime de Stokes dans un espace annulaire," Mech. Res. Commun. **28**, 113 (2001).
[15] T. S. Krasnopolskaya, V. V. Meleshko, G. W. M. Peters, and H. E. H. Meijer, "Mixing in Stokes flow in an annular wedge cavity," Eur. J. Mech. B/Fluids **18**, 793 (1999).
[16] V. V. Meleshko and H. Aref, "A blinking rotlet model for chaotic advection," Phys. Fluids **8**, 3215 (1996); erratum, *ibid.* **10**, 1543 (1998).
[17] D. G. Crowdy, A. Surana, and K.-Y. Yick, "Irrotational motion generated by two planar stirrers in inviscid fluid," Phys. Fluids **19**, 018103 (2007).